analytical chemistry

Article

pubs.acs.org/ac

Isoelectric Focusing in a Silica Nanofluidic Channel: Effects of Electromigration and Electroosmosis

Wei-Lun Hsu,[†] David W. Inglis,[‡,§] Michael A. Startsev,[‡] Ewa M. Goldys,[§] Malcolm R. Davidson,[†] and Dalton J.E. Harvie*[,†]

[†]Department of Chemical and Biomolecular Engineering, University of Melbourne, Parkville, Victoria 3010, Australia

[‡]Department of Engineering and [§]MQ BioFocus Research Centre, Macquarie University, Sydney, New South Wales 2109, Australia

Supporting Information

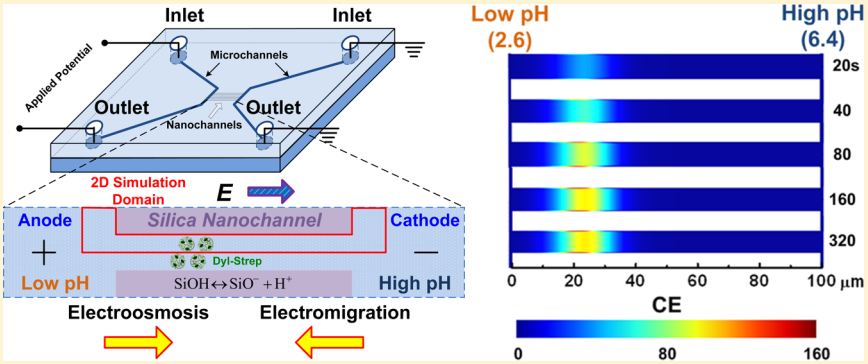

ABSTRACT: Isoelectric focusing of proteins in a silica nanofluidic channel filled with citric acid and disodium phosphate buffers is investigated via numerical simulation. Ions in the channel migrate in response to (i) the electric field acting on their charge and (ii) the bulk electroosmotic flow (which is directed toward the cathode). Proteins are focused near the low pH (anode) end when the electromigration effect is more significant and closer to the high pH (cathode) end when the electroosmotic effect dominates. We simulate the focusing behavior of Dylight labeled streptavidin (Dyl-Strep) proteins in the channel, using a relationship between the protein's charge and pH measured in a previous experiment. Protein focusing results compare well to previous experimental measurements. The effect of some key parameters, such as applied voltage, isoelectric point (pI), bulk pH, and bulk conductivity, on the protein trapping behavior in a nanofluidic channel is examined.

Isoelectric focusing (IEF) of proteins is becoming an irreplaceable tool for proteomics. The earliest documented concentration of proteins in a pH gradient that utilized a protein's isoelectric point (pI, the specific pH at which the electrophoretic mobility of an amphoteric particle equals zero), occurred in the midfifties when Kolin separated hemoglobin from cytochrome in a glycerol solution.[1] The method relies on the uniqueness of pIs for ampholytes, such as proteins, peptides and amino acids: Different molecules, with different density and equilibrium constant of functional groups, are focused at different pH positions. When an electric field parallel to the pH gradient direction is applied, molecules whose pI is lower/higher than the local pH migrate toward the anode/cathode. Molecules keep moving until the pH reaches their pI, at which point the electrophoretic force on the molecules is zero.

Kolin's[1] apparatus and other such traditional IEF devices are conducted in devices that are large enough that boundary effects are insignificant. Conducting IEF in small capillaries (cIEF) provides some advantages over these traditional techniques, such as the improved dissipation of Joule heat, better separation resolution, and much shorter analysis times.[2,3] Micro Total Analysis Systems (μTAS), also known as "lab-on-a-chip" devices (LOC),[4] are now also being employed. Similar to cIEF, reduced sample consumption, low cost, high resolution, and short detection times are some of the potential benefits of microfluidic chip-based isoelectric focusing (μIEF) systems. Additionally, microchannels are easy to integrate with other microsystem units, facilitating complex (parallel) device design and corresponding enhanced analyte throughput.

In conjunction with the advantages offered by these smaller scale devices, the electric charge at the boundary surface adds complexity to the operating and analysis of cIEF and μIEF. Because of its abundance, low cost and material integrity, one of the most commonly used materials for capillary and microfluidic channels is silica. The silica surface is charged when exposed to an aqueous solution because of the protonation or deprotonation of the surface amphoteric silanol groups.[5] Most IEF is conducted at pH > 2.5, because of the carrier ampholyte availability and because the pI of most targeted biomolecules are located in this range. As deprotona-

Received: May 19, 2014
Accepted: August 6, 2014
Published: August 6, 2014

tion is the dominant effect at these pH levels, the surface is negatively charged throughout. Only when the bulk solution is extremely acidic (pH < 2) is the protonation effect stronger than deprotonation, giving a positively charged surface.[6,7] The surface charge induces an electric double layer (EDL) in the vicinity of the channel walls, which in turn induces an electroosmotic flow when a tangential (to the surface) electric field is applied along the channel. This significantly influences cIEF and μIEF behavior.[8,9]

Neutral hydrophilic polymer coatings applied to silica surfaces can suppress the electroosmotic flow;[10,11] however, the coatings can also hinder some inherent advantages, such as high UV transparency and smoothness.[11] For instance, a generally used polymer coating material, hydroxylpropylmethyl cellulose, has a strong propensity to absorb blue light resulting in slightly yellow colored films.[12] Also, while the average roughness of hydroxylpropylmethyl cellulose is within the range of several hundred nanometers[12] (and may be insignificant in microscale devices), this scale is an important issue in nanofluidic devices. An alternative to preventing electroosmotic flow is to use gel matrices within the channels. The original motivation for employing these immobile pH gradients (IPG) was to eliminate contamination of buffer ions on proteins: For example, Bjellqvist et al.[13] used a cross-linked polyacrylamide (PA) matrix. Such applied physical columns largely suppress electroosmotic flow, however they must be separately inserted into integrated LOC devices adding cost and hindering downstream processing.

Even though cIEF and μIEF are powerful separation techniques that have been broadly used in analytical chemistry, the ionic behavior within these systems is not well understood. For example, different degrees of pH gradient compression can occur as a function of time and voltage. In some systems, the pH gradient drifts toward the cathodic end and vanishes (the pH plateaus) at the anodic end in a phenomenon known as "cathodic drift".[14,15] In other systems the pH distribution experiences "anodic drift", meaning that the pH gradient relocates toward the anodic end.[14,16] The carrier ampholyte composition and concentration ratio of anolyte and catholyte determine which drift is dominant. While the mechanism of these phenomena is complex and not fully understood, it is speculated that electroosmosis, electromigration, and electrolyte diffusion all play roles.[14,17,18]

Hence, to further advance the cIEF and μIEF techniques, investigation of the ionic behavior within these systems is required. Over the last two decades, analytical and computational studies have been widely used to study electroosmotic and electrophoretic behavior in larger scale IEF.[19−24] Herr et al.[19] investigated the electroosmotic velocity and sample-dispersion rate in a cylindrical capillary comprised of two distinct zeta potential regions using an analytical method. Using finite volume methods with structured grids, Chatterjee[20] constructed a numerical model of a complex three-dimensional (3D) mixer. Both electroosmotic flow and IEF of Histidine in an immobilized pH gradient composed of cacodylic acid (CACO) and tris(hydroxymethyl)-aminomethane (TRIS) in a straight microchannel were examined. Lam et al.[21] employed both analytical and finite element models to study IEF of peptides in multicompartment free-flow microchannels above an immobilized pH gradient (IPG) gel (OFFGEL IEF). Shim et al.[22] used a two-dimensional (2D) finite volume model to investigate IEF by considering (i) IEF in a CACO/TRIS IPG gel; (ii) IEF in a 10 carrier-ampholyte environment in a straight channel; and (iii) IEF in a 10 carrier-ampholyte environment in a contraction−expansion channel. Estimating the electroosmotic mobility as a function of ionic strength and pH based on previous experimental results, Thormann et al.[23] simulated IEF in bare fused silica (FS), surface sulfonated polymer coated fused silica, poly(methyl methacrylate) (PMMA) and polydimethylsiloxane (PDMS) capillaries and microchannels. Kler et al.[24] used a 3D time-dependent numerical model based on a finite element scheme to investigate free flow IEF and capillary zone electrophoresis in a 2D electrophoretic separation geometry.

In these and similar studies on IEF, the focus has been on micro- or larger scales where the EDL thickness is small compared to the depth of the channels (for binary and monovalent ionic systems such as NaCl solutions, the Debye length is 3.04×10^{-4} and 9.63×10^{-2} μm at 1 and 10^{-5} M, respectively). At these large scales, the free slip Helmholtz−Smoluchowski boundary condition can be applied and the electroosmotic flow variation within the EDL neglected.[25] When the channel size shrinks to the nanoscale, however, the EDL thickness becomes comparable to the channel depth and the flow variation within the EDL becomes important to predicting the performance of the device.

Recently, Startsev et al.,[26] for the first time, demonstrated free flow IEF of proteins, *R*-phycoerythrin (*R*-PE) and Dylight labeled streptavidin (Dyl-Strep), in a fused-silica nanofluidic channel without a polymer coating surface modification. They used a pH gradient established by mixing various volumes of citric acid and disodium orthophosphate buffers that were continuously circulated through microchannels attached to each end of the nanochannel. More analysis is needed to understand the electroosmotic and focusing behavior in this nanofluidic device. Here, we use numerical methods to computationally simulate pH gradient electrofocusing in Startsev's system. The large aspect ratio (length/depth) nanochannel problem that involves multiple chemical reactions is solved using an implicit finite volume method.[27] The distributions of pH gradient and electroosmotic behavior along a nanofluidic channel at different focusing times, applied voltage, bulk pH, bulk conductivity, and the trapping behavior of proteins with different isoelectric points are examined.

THEORY

As illustrated in Figure 1, a nanofluidic system composed of two silica microchannels connected via a nanochannel array is considered. Experimentally[26] the channels have both straight and tapered widths within the central array, however we only consider the purely rectangular nanochannels here with 20 μm width, 100 μm length and 85 nm depth. We select the effective number of parallel, rectangular nanochannels (M)[28] within the array as 14 in our simulations, to achieve approximate correspondence between trap locations measured in the experiment and found computationally. Note that M is the sole semifree parameter used in the simulations. It affects the potential drop applied over the nanochannel via an electrokinetic circuit analysis that models the flows and potential drops within the connected microchannels, as detailed in Supporting Information SI 1. Each microchannel carries an incompressible Newtonian electrolyte solution circulated continuously to maintain the pH gradient. The left microchannel has a lower pH solution compared to the right microchannel. In the previous experiments[26] solutions were prepared by mixing different volume ratios of 0.1 M citric acid

dx.doi.org/10.1021/ac501875u | Anal. Chem. 2014, 86, 8711−8718

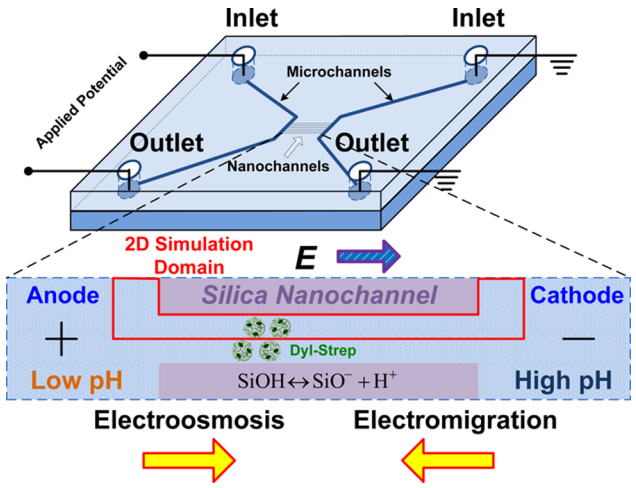

Figure 1. Schematic diagram of the nanofluidic device.

$C_6H_8O_7$ and 0.2 M disodium orthophosphate Na_2HPO_4 electrolytes. In the low pH solution, citric acid was the dominant species while phosphoric acid was dominant in the high pH solution. Sodium chloride and deionized water were added to offset the conductance difference between the two solutions. If solution conductance was higher/lower than the targeted conductance, deionized water/sodium chloride was added. The targeted conductance was the conductance of the buffer solution mixture at pH = 6.6 before adding any sodium chloride or deionized water (4.6 mS/cm, measured experimentally).[26] The positive electrodes (anode) were connected to both ends of the low pH microchannel while the negative electrodes (cathode) were connected to both ends of the high pH microchannel, producing an electric field directed toward the high pH end of the nanochannels.

The solute concentration, electric potential, and electroosmotic flow distributions are obtained by solving the following coupled steady-state partial differential equations: The electric Poisson equation, continuity equation, modified Navier–Stokes equation (containing an electric body force source term and nonuniform viscosity) and modified Nernst–Planck equations (containing a reaction term).

$$\epsilon\epsilon_0\nabla^2\phi = -\rho_e \tag{1}$$

$$\nabla\cdot\mathbf{v} = 0 \tag{2}$$

$$\rho\nabla\cdot\mathbf{vv} = -\nabla p + \nabla\cdot\mu\nabla\mathbf{v} - \rho_e\nabla\phi \tag{3}$$

$$\nabla\cdot\mathbf{j}_i = S_i \tag{4}$$

In these expressions, ϕ, ρ, ρ_e, ϵ, ϵ_0, $\mathbf{v}$, μ, and p are the electric potential, density of the liquid phase, space charge density, dielectric constant,permittivity of vacuum, velocity, viscosity, and pressure, respectively. $\mathbf{j}_i$ and S_i are the flux and reaction source of species i, respectively. Because of the polarization of water molecules, the solvent viscosity is influenced by the local electric field magnitude, referred to as the viscoelectric effect:[29]

$$\mu = \mu_0(1 + f|\mathbf{E}|^2) \tag{5}$$

Here, μ_0, f, and $\mathbf{E}$ $(= -\nabla\phi)$ are the solvent viscosity in the absence of the electric field, viscoelectric coefficient and local electric field, respectively. In this simulation, we adopt the viscoelectric coefficient of water $(1 \times 10^{-15}\ m^2/V^2)$, measured experimentally,[30] which is consistent with the value estimated theoretically by Lyklema and Overbeek.[29] The flux of species i, $\mathbf{j}_i$, is the sum of the advection, diffusion and conduction terms:

$$\mathbf{j}_i = n_i\mathbf{v} - \mathcal{D}_i\left(\nabla n_i + \frac{z_i e}{k_B T}n_i\nabla\phi\right) \tag{6}$$

where $\mathcal{D}_i$, z_i, and n_i are the diffusivity, valence, and concentration of species i, respectively. k_B, T, and e are the Boltzmann constant, absolute temperature, and elementary charge, respectively. $\mathcal{D}_i$, z_i, and S_i are summarized in Supporting Information SI 2.

The same amount of Dyl-Strep proteins are added to the buffer solutions of both microchannels. In the simulations, we assume that (i) the charge attributed by proteins is much lower than those from the buffer solutions, which is valid when the protein concentration is dilute compared to the solute concentrations, and (ii) the steric effect of proteins is ignored with the molecules being regarded as point charges. Assumption (i) allows the background electrolyte flow to be solved independently from the protein transport, which is solved using a transient modified Nernst–Planck equation (with a conduction term):

$$\frac{\partial n_{\text{Dyl-Strep}}}{\partial t} + \nabla\cdot\left[n_{\text{Dyl-Strep}}\mathbf{v} - \mathcal{D}_{\text{Dyl-Strep}}\left(\nabla n_{\text{Dyl-Strep}} + \frac{z_{\text{Dyl-Strep}}e}{k_B T}n_{\text{Dyl-Strep}}\nabla\phi\right)\right] = 0 \tag{7}$$

Here, $n_{\text{Dyl-Strep}}$, $\mathcal{D}_{\text{Dyl-Strep}}$, and $z_{\text{Dyl–Strep}}$ are the concentration, diffusivity, and charge of Dyl-Strep, respectively, and t denotes time. The diffusivity of quasi-spherical Dyl-Strep molecules is derived (bulk value of 8.74×10^{-11} m^2/s) based on the Stokes–Einstein equation with the molecule radius $R_{\text{Dyl-Strep}}$ = 2.5 nm obtained from the RCSB Protein Data Bank,[31] namely

$$\mathcal{D}_{\text{Dyl-Strep}} = \frac{k_B T}{6\pi\mu R_{\text{Dyl-Strep}}} \tag{8}$$

Similar to most biomolecules, Dyl-Strep is a kind of amphoteric species which has both deprotonation and protonation functional groups. These functional groups can release and/or accept protons in electrolytes and thus the net molecular charge depends on the local concentration of the proton, that is, the local pH. Molecules are positively charged at low pH: On the other hand, deprotonation is dominant when the proton concentration is low, so the molecules have a tendency to be negatively charged. At the isoionic point, the charge from protonation is offset by that from deprotonation and hence the molecules become zwitter-molecules (electric neutral). In practice, one biomolecule can be comprised of multiple deprotonation and protonation functional groups and each group can release/accept multiple protons. For simplicity, we assume each Dyl-Strep molecule possesses only one monodeprotonation (HA) and one monoprotonation (BOH) functional group, namely

$$\text{HA} \leftrightarrow \text{A}^- + \text{H}^+;\ K_a = \frac{[\equiv\text{A}^-]n_{\text{H}+}}{[\equiv\text{HA}]} \tag{9}$$

$$\text{BOH} + \text{H}_2\text{O} \leftrightarrow \text{BOH}_2^+ + \text{OH}^-;\ K_b = \frac{[\equiv\text{BOH}_2{}^+]n_{\text{OH}^-}}{[\equiv\text{BOH}]} \tag{10}$$

dx.doi.org/10.1021/ac501875u | Anal. Chem. 2014, 86, 8711–8718

Here, [≡HA], [≡A$^-$], [≡BOH], and [≡BOH$_2^+$] are the surface density of HA, A$^-$, BOH, BOH$_2^+$ functional groups on the protein molecule, respectively. K_a and K_b are the equilibrium constant of deprotonation and protonation, respectively. The charge of a protein molecule $z_{Dyl-Strep}$ can then be expressed as

$$z_{Dyl\text{-}Strep} = -\Gamma_a \frac{K_a}{K_a + n_{H+}} + \Gamma_b \frac{K_b n_{H+}}{1 + K_b n_{H+}} \quad (11)$$

where Γ_a and Γ_b are the number of deprotonation and protonation functional groups on a Dyl-Strep molecule, respectively. By using previous experimentally measured values on $z_{Dyl\text{-}Strep}$ between pH = 2.5 and 6.6, we find values of Γ_a, pK_a, Γ_b, and pK_b that reproduce the experimentally observed charge and pH relationship, as shown in Figure 2. Hence, the simplification represented by eqs 9 and 10 appears to be justified.

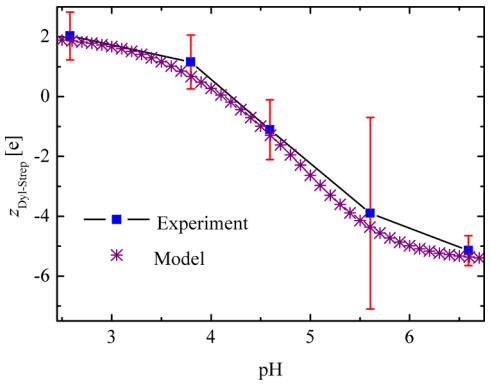

Figure 2. Charge of Dyl-Strep $z_{Dyl\text{-}Strep}$ as a function of pH. The blue square symbols are the experimental values;[26] the purple crosses are the theoretical predictions based on the employed simulation values of Γ_a = 5.5, pK_a = 5, Γ_b = 2, and pK_b = −3.8.

The coupled partial differential equations, eqs 1−4 and 7 are solved with the associated initial condition and boundary conditions detailed in Supporting Information SI 3. We analyze Dyl-Strep pH gradient electrofocusing behavior in a nanochannel by estimating the trap locations and concentration enhancement factor (CE), which is defined as the local Dyl-Strep concentration in the nanochannels divided by the input Dyl-Strep concentration in microchannels:

$$CE = \frac{n_{Dyl\text{-}Strep}}{n_{Dyl\text{-}Strep,input}} \quad (12)$$

RESULTS AND DISCUSSION

In this nanofluidic trapping system, the proteins are supplied into the nanochannels from both the high and low pH microchannels (Figure 1). In the low pH microchannel, the high proton concentration ensures that the proteins are positively charged. The applied electric field drives all positively charged molecules toward the cathode (the high pH end) generating an influx of proteins into the nanochannels from the low pH microchannel. Conversely, the proteins in the high pH microchannel are negatively charged because of the dilute proton concentration there, and hence the applied field causes these proteins to migrate toward the anode (the low pH end) via the nanochannels. Concurrently, the electroosmotic flow in the nanochannels due to the electric force from the applied tangential electric field on the positively charged solution within the EDL (the silica surface is negatively charged) is directed from the low pH end to high pH end, increasing the positively charged proteins migration speed but hindering the movement of the negatively charged proteins.

Effect of Focusing Time. CE as a function of focusing time is shown in Figure 3. The CE and trap location (at nanochannel position ∼25 μm) closely match the experimental results.[26] Both experimental and theoretical results show that the CE increases rapidly in the first 100 s before saturating at ∼200 s. The protein concentration is governed by advection, diffusion and conduction forces, as detailed in eq 7. As the CE rises, the diffusion force, which opposes accumulation, becomes significant and, balances the advection and conduction forces, eventually achieving a steady-state. Note that in the contours of the protein focusing in the nanochannels (Figure 3c), an apparent adsorption of proteins (red area) on the silica nanochannel surface is visible. The isoionic point of silica in aqueous solution is pH ∼ 2 which is lower than the present pH levels (2.6−6.4). Therefore, the silica surface is negatively charged throughout the device so that the positively charged proteins (to the left of the trap location) are attracted/adsorbed onto the negatively charged silica surface, while the negatively charged proteins (to the right of the trap location) are repelled from the surface. The maximum values of the CE near the silica surface and that near the centerline of the nanochannel are at slightly different axial locations because the local electroosmotic velocity near the surface is weaker than that near the nanochannel centerline. This may result in two peaks of depth averaged CE along the nanochannel if this adsorption effect is significant. In the present applied voltage range (0−0.4 V), only one peak of depth averaged CE is observed (from the protein concentration near the centerline) implying that adsorption is marginal. However, a distorted and nonuniform trapping band was observed in the experiment[26] when the applied voltage was significantly large (3 V), suggesting that this type of adsorption may be a potential issue for this technique.

Effect of Isoelectric Point (pI). To demonstrate separation in this device, we simulate a second model protein within the channel that has a higher pI. Figure 4 shows the results. The pIs (see subfigure) for the proteins A and B are ∼4.1 and 5.9, respectively. [Note that in the simulations, a protein's EDL is neglected (whereby the proteins are regarded as point charges) so that the isoionic point and pI of proteins are equal.] The protein A is focused closer to the low concentration end (the peak position is at ∼23 μm in contrast to ∼43 μm for the protein B) which is attributed to its lower pI. Note that the average value for the bulk pHs from the two ends is 4.5 [(2.6 + 6.4)/2] which is lower than the pI for the protein B. If the pH distribution in the channel were linear, protein B would be trapped closer to the high pH end of the channel (i.e., within 50−100 μm). That it is not implies that the pH gradient in the channel has shifted toward the low concentration end (anodic drift). In the following subsections (Effect of Applied Voltage, Effect of Bulk pH, and Effect of Bulk Conductivity sections), we examine the trap locations for Dyl-Strep and pH distribution in the channel length's direction at different conditions to understand the mechanism of this drift.

Effect of Applied Voltage. The trap locations and pH gradients within a nanofluidic channel are functions of the applied electric potential, as shown in Figure 5. Interestingly, the CE does not change monotonically with applied electric

dx.doi.org/10.1021/ac501875u | Anal. Chem. 2014, 86, 8711−8718

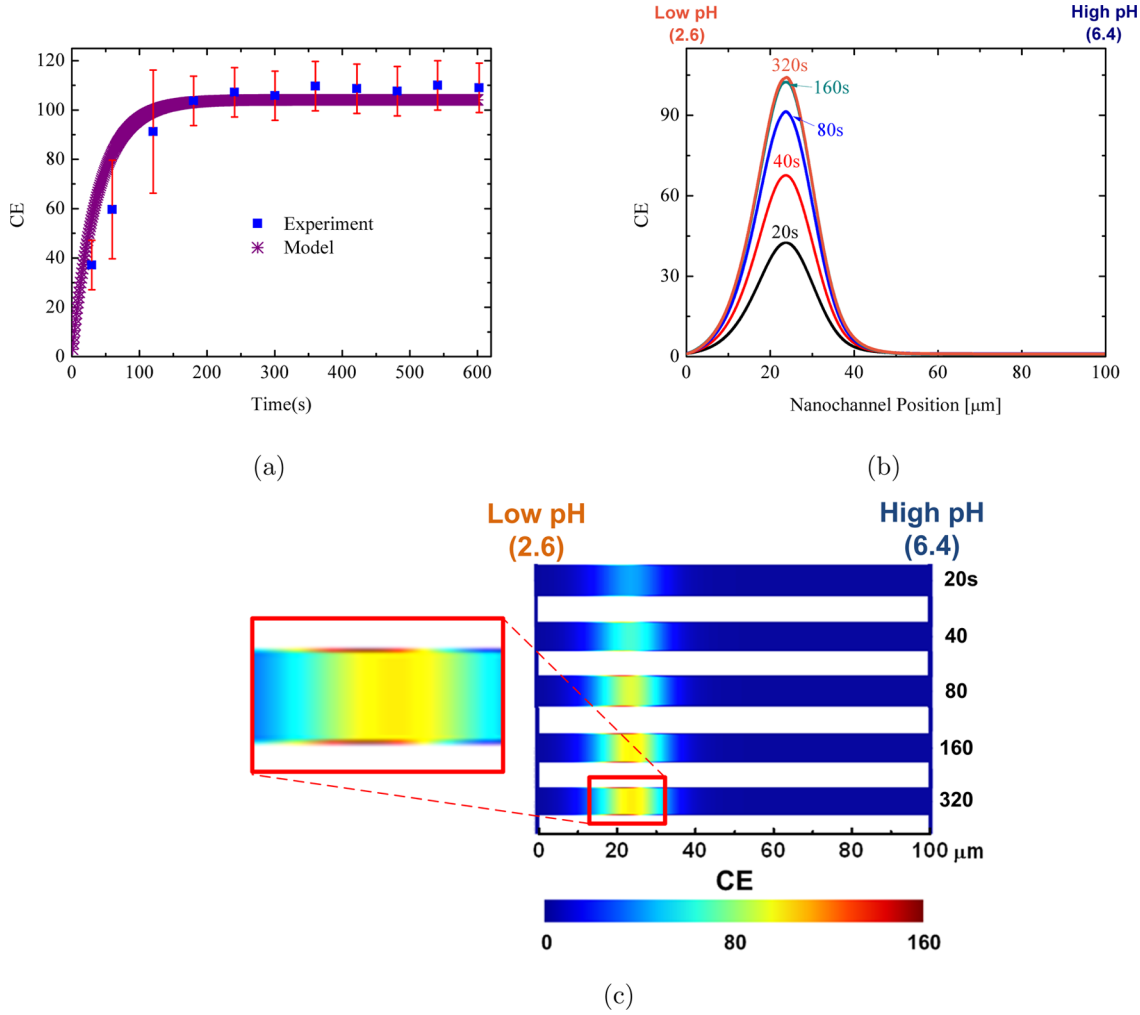

Figure 3. Variations of Dyl-Strep concentration enhancement (CE) as a function of time at pH = 2.6 in the left microchannel and 6.4 in the right microchannel: (a) time versus maximum depth averaged CE in a nanofluidic channel. The blue square symbols are the experimental values;[26] the purple spots are the theoretical estimations. (b) Nanochannel position in the axial direction (0 and 100 μm stand for the low and high pH ends, respectively) versus CE on the centerline of a nanofluidic channel; (c) contours of CE across the depth of a nanofluidic channel at different time periods (exaggerated 235 times in nanochannel depth direction).

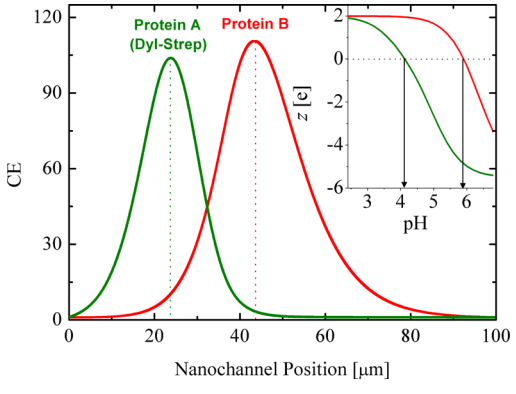

Figure 4. Variations of concentration enhancement (CE) for two types of protein with the same radius (2.5 nm) but different charge conditions (A is Dyl-Strep with Γ_a = 5.5, pK_a = 5, Γ_b = 2, and pK_b=−3.8 and B is a protein with Γ_a = 5.5, pK_a = 6.5, Γ_b = 2, and pK_b = −6) as a function nanochannel position at pH = 2.6 in the left microchannel and 6.4 in the right microchannel at t = 10 min. Inset: Variations of protein charge z as a function of pH for proteins A and B.

potential and reaches a maximum value when the peak location is at around 40 μm along the nanochannel axis (with 0 and 100 μm representing for the low and high pH ends, respectively). The trap drifts to the low pH end (anode) as the applied electric potential increases. Also, the maximum CE increases sharply with electric potential when the potential is lower than a critical value (~0.3 V when the CE reaches a maximum), but decreases gradually again when the potential is greater than this value. The pH distributions along the centerline of the nanochannel reveal that the drift of the trap location is attributed to the migration of pH gradients and the critical point occurs when the pH distribution is close to a linear function of nanochannel position. The pH distribution drift is opposite to the direction of the electroosmotic flow (which is from the left to right), so is not a direct consequence of convective or electric (conductive) proton migration as it was in previous work using a conductivity gradient.[28,32] Rather, as shown by the concentration distributions of all buffer species along the centerline of a nanochannel at two different applied electric potentials (Figure 6), there is an anodic drift of all ionic buffer species (anions) toward the low pH end (anode) when the applied electric potential increases. It is this bulk anionic

dx.doi.org/10.1021/ac501875u | Anal. Chem. 2014, 86, 8711−8718

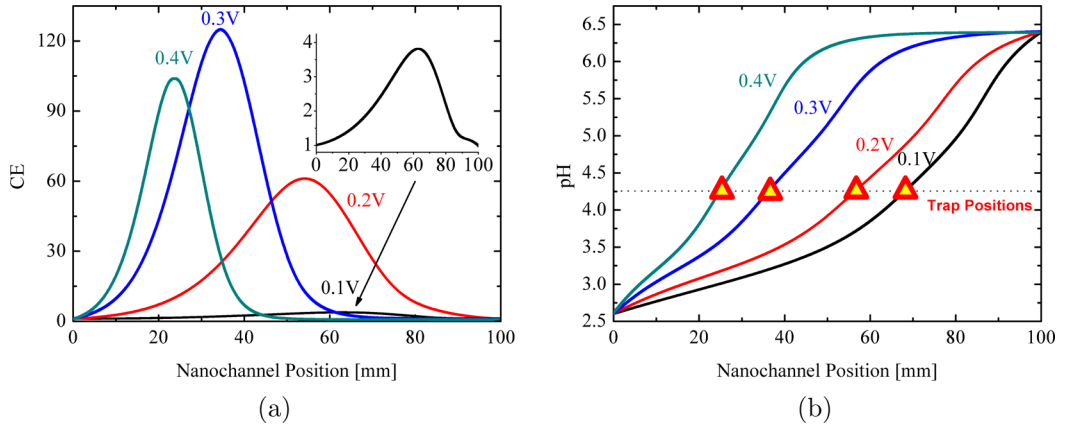

Figure 5. Variations of (a) Dyl-Strep concentration enhancement (CE) (b) local pH along the nanochannel centerline at different levels of applied electric potentials at pH = 2.6 in the left microchannel and 6.4 in the right microchannel.

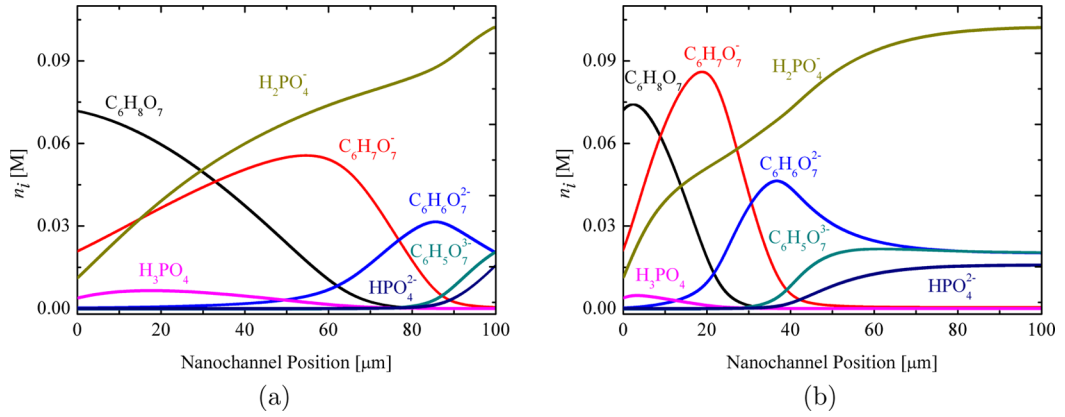

Figure 6. Buffer group concentrations along the nanochannel centerline at pH = 2.6 in the left microchannel and 6.4 in the right microchannel with applied electric potential = (a) 0.1 and (b) 0.4 V.

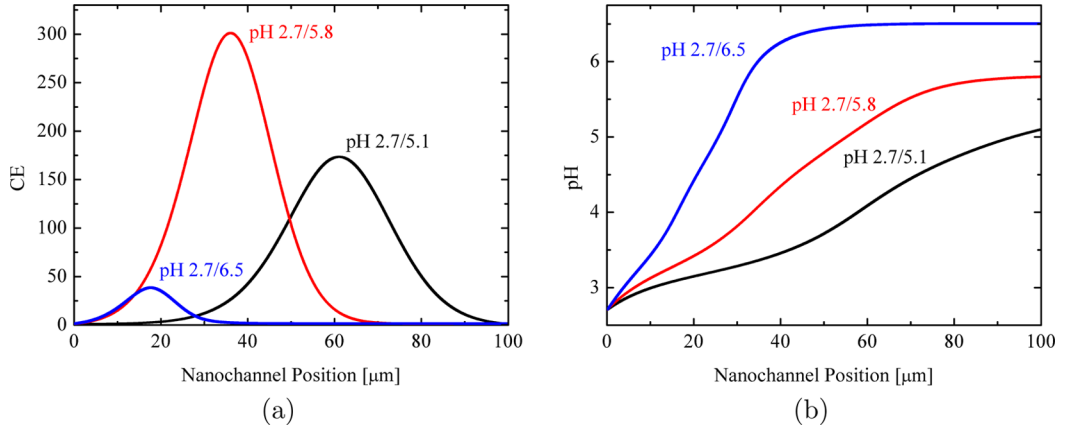

Figure 7. Variations of (a) Dyl-Strep concentration enhancement (CE) (b) local pH along the nanochannel centerline at different bulk pH values (5.1, 5.8, and 6.5) in the high pH microchannel (pH = 2.7 in the low pH microchannel) at the applied electric potential = 0.4 V.

electromigration that drives the drift of pH gradient, and thus the trap location, as the electric potential changes.

Effect of Bulk pH. Another way to manipulate the trap locations is to directly change the bulk pH by mixing different proportions of citric acid and disolium orthophosphate used in the microchannels. As demonstrated in Figure 7, the trap location for Dyl-Strep moves to the high concentration end as the pH in the high pH microchannel decreases, as expected. There appears to be an optimal pH range that gives the highest CE.

One of the reasons for choosing pH values in the two microchannels that are close to each other is to optimize separation performance. The magnitude of the pH gradient decreases as the pH difference between the two microchannels decreases, yielding more discriminative traps for different kinds of proteins (i.e., giving a wider separation band). This approach is suitable for separating proteins having similar pIs, such as *R*-

dx.doi.org/10.1021/ac501875u | *Anal. Chem.* 2014, 86, 8711−8718

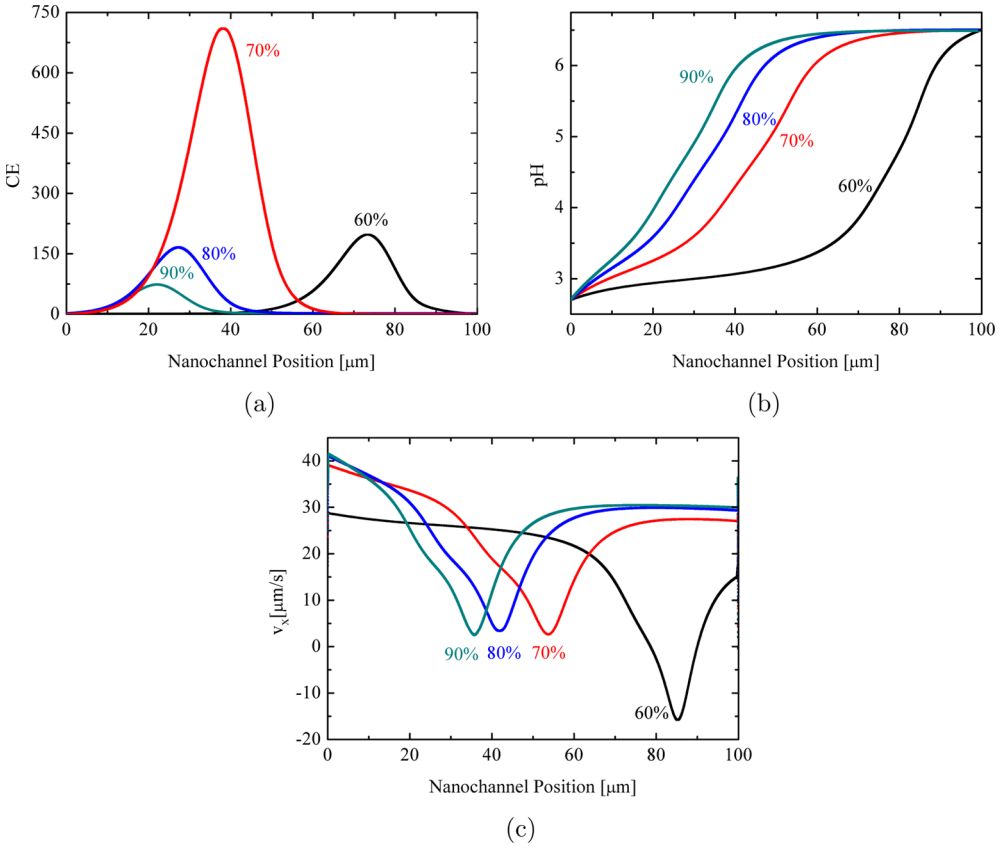

Figure 8. Variations of (a) Dyl-Strep concentration enhancement (CE) (b) local pH (c) axial electroosmotic velocity v_x on the centerline at different solution conductivities (90, 80, 70 and 60% of the original conductivity at pH = 6.6) at pH = 2.7 in the left microchannel and 6.5 in the right microchannel.

PE and Dyl-Strep. However, if the proteins to be separated have very different pIs, a small pH gap may not be able to capture all of the targeted proteins and a wide pH band is needed.

Effect of Bulk Conductivity. To suppress the effect of electroosmotic flow on the trapping technique, the experiment[26] was conducted using high conductivity solutions. However, it may be possible to use electrosmotic flow to increase the CE and enlarge the separation band by creating a pH distribution in the nanochannel that is closer to a linear function of nanochannel position (in the axial direction). Electroosmotic flow is a function of the EDL thickness (the Debye length) which is inversely proportional to the bulk ionic strength. When the ionic strength is high (the EDL thickness is thin), the volume of charged solution is small and located very close to the channel surface: This fluid suffers from a significant friction force, yielding low electroosmotic flow. As the ionic strength decreases, the EDL thickness increases, increasing the volume of charged fluid within the channel (which is now further from the wall) and increasing the electroosmotic flow. However, if the ionic strength is too low, decreasing the ionic concentration further results in a smaller electroosmotic flow due to a weaker space charge within the EDL.

Figure 8 shows the CE, pH, and electroosmotic velocity in a nanochannel at four different conductivities (expressed as a proportion of the conductance at pH = 6.6, that is, before adding any sodium chloride or deionized water). In the present conductivity range (100−60%), the electroosmotic effect increases with an increase in the EDL thickness. Hence, as the conductivity decreases, both the traps and pH gradients are pushed toward the high pH end (cathode) of the nanochannels by the electroosmotic flow. The CE reaches a maximum value at a medium conductivity (70%). It is interesting to see that the centerline electroosmotic velocity profile is not constant along the nanochannel axial direction (shown in Figure 8c), which differs from previous understanding.[26] When the pH increases, two electroosmotic driving forces compete to produce this variation; (i) the increase of the silica surface charge density, and (ii) the decrease of the EDL thickness. The former is due to the deprotonation of the silica surface that is favorable at high pH, and increases the local electroosmotic flow near the silica surface. The latter: Although the conductivity is constant in the two microchannels, the ionic strength is higher in the high pH microchannel, yielding a thinner EDL at the high pH end which depresses the local electroosmotic flow near the silica surface (see Supporting Information SI 4). To further complicate the situation, the flow within the nanochannel is constrained by mass conservation, producing a nonuniform pressure gradient along the nanochannel's length.[33] The net effect in the present system is to produce velocity profiles as indicated in Figure 9. Note that the flow at the centerline in the nanochannel reverses in the 60% case. A similar observation was found in a previous study of pH gradient electrokinetic transport in microcapillaries.[34] Such flow recirculations may significantly affect trapping performance.

■ CONCLUSION

Isoelectric focusing of Dyl-Strep is investigated by considering the electrophoretic and electroosmotic behavior of amphoteric

dx.doi.org/10.1021/ac501875u | Anal. Chem. 2014, 86, 8711−8718

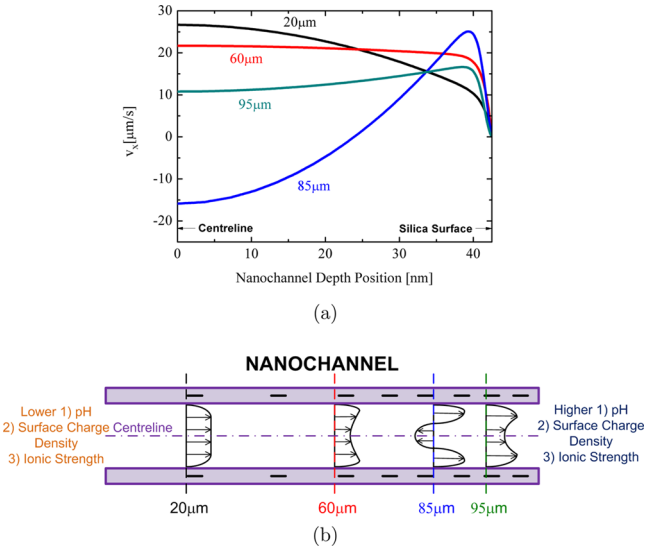

Figure 9. (a) Electroosmotic velocity profiles in the nanochannel depth direction (0 and 42.5 nm stand for the centerline and silica surface of the nanochannel) at different nanochannel positions in the axial direction and conductivity = 60% of the original conductivity, pH = 2.7 in the left microchannel and 6.5 in the right microchannel; (b) a schematic diagram of the electroosmotic velocity profile along the nanochannel at conductivity = 60% of the original conductivity.

molecules in silica nanofluidic channels filled with a controlled gradient of citric acid and disodium orthophosphate buffer solutions. The simulated concentration enhancement (CE) closely matches both transient and steady-state experimental data. The effects of focusing time, pI, applied voltage, bulk pH and bulk conductivity on the traps and pH gradients are examined theoretically. Electromigration drives the traps toward the anode (the low pH end) while electroosmosis pushes the traps toward the cathode (the high pH end). The protein trapping CE increases rapidly in the first 100 s and reaches a steady-state within approximately 3 min. The trap locations are closer to the low pH end at the larger applied electric potential. The CE reaches a maximum value when the trap location is at around 40 μm from the low pH end in the nanochannel. Protein adsorption like behavior is observed on the nanochannel surface near the trap location. The trap location drifts to the high pH end when the pH in the high pH microchannel is lower or the bulk solution conductivity is lower. The electroosmotic velocity profile in the silica nanofluidic channel is nonuniform and a local recirculating flow is formed when the bulk solution conductivity is low.

■ ASSOCIATED CONTENT

Ⓢ Supporting Information

Additional material as described in the text. This material is available free of charge via the Internet at http://pubs.acs.org.

■ AUTHOR INFORMATION

Corresponding Author

*E-mail: daltonh@unimelb.edu.au. Phone: +61 3 8344 6421. Fax: +61 3 8344 4153.

Notes

The authors declare no competing financial interest.

■ ACKNOWLEDGMENTS

This work was supported by the Australian Research Council (DP110102207).

■ REFERENCES

(1) Kolin, A. *J. Chem. Phys.* **1954**, *22*, 1628−1629.
(2) Pritchett, T. *Electrophoresis* **1996**, *17*, 1195−1201.
(3) Righetti, P. G.; Sebastiano, R.; Citterio, A. *Proteomics* **2013**, *13*, 325−340.
(4) Reyes, D.; Iossifidis, D.; Auroux, P.; Manz, A. *Anal. Chem.* **2002**, *74*, 2623−2636.
(5) Behrens, S.; Grier, D. *J. Chem. Phys.* **2001**, *115*, 6716.
(6) Hiemstra, T.; Dewit, J.; Vanriemsdijk, W. *J. Colloid Interface Sci.* **1989**, *133*, 105−117.
(7) Behrens, S.; Borkovec, M. *J. Phys. Chem. B* **1999**, *103*, 2918−2928.
(8) Stern, O. *Z. Elektrochem.* **1924**, *30*, 508−516.
(9) Grahame, D. *Chem. Rev.* **1947**, *41*, 441−501.
(10) Righetti, P.; Gelfi, C.; Conti, M. *J. Chromatogr. B* **1997**, *699*, 91−104.
(11) Silvertand, L. H. H.; Torano, J. S.; van Bennekom, W. P.; de Jong, G. J. *J. Chromatogr. A* **2008**, *1204*, 157−170.
(12) Villalobos, R.; Chanona, J.; Hernandez, P.; Gutierrez, G.; Chiralt, A. *Food Hydrocolloid.* **2005**, *19*, 53−61.
(13) Bjellqvist, B.; Ek, K.; Righetti, P.; Gianazza, E.; Gorg, A.; Westermeier, R.; Postel, W. *J. Biochem. Biophys. Methods* **1982**, *6*, 317−339.
(14) Mosher, R.; Thormann, W. *Electrophoresis* **1990**, *11*, 717−723.
(15) Xu, Z.; Okabe, N.; Arai, A.; Hirokawa, T. *Electrophoresis* **2010**, *31*, 3558−3565.
(16) Nguyen, N.; Mccormick, A.; Chrambach, A. *Anal. Biochem.* **1978**, *88*, 186−195.
(17) Righetti, P. G. *Isoelectric Focusing: Theory, Methodology and Applications*, ed.; Elsevier Biomedical: Amsterdam, 1983.
(18) Sommer, G. J.; Hatch, A. V. *Electrophoresis* **2009**, *30*, 742−757.
(19) Herr, A.; Molho, J.; Santiago, J.; Mungal, M.; Kenny, T.; Garguilo, M. *Anal. Chem.* **2000**, *72*, 1053−1057.
(20) Chatterjee, A. *J. Micromech. Microeng.* **2003**, *13*, 758−767.
(21) Lam, H.-T.; Josserand, J.; Lion, N.; Girault, H. H. *J. Proteome Res.* **2007**, *6*, 1666−1676.
(22) Shim, J.; Dutta, P.; Ivory, C. F. *Electrophoresis* **2007**, *28*, 572−586.
(23) Thormann, W.; Caslavska, J.; Mosher, R. A. *J. Chromatogr. A* **2007**, *1155*, 154−163.
(24) Kler, P. A.; Berli, C. L. A.; Guarnieri, F. A. *Microfluid. Nanofluid.* **2011**, *10*, 187−198.
(25) Masliyah, J.; Bhattacharjee, S. *Electrokinetic and Colloid Transport Phenomena*, 4th ed.; John Wiley: Hoboken, NJ, 2006.
(26) Startsev, M. A.; Inglis, D. W.; Baker, M. S.; Goldys, E. M. *Anal. Chem.* **2013**, *85*, 7133−7138.
(27) Harvie, D. J. E. arb. http://people.eng.unimelb.edu.au/daltonh/downloads/arb/code/latest/examples/electrokinetic_channel_flow/.
(28) Hsu, W.-L.; Inglis, D. W.; Jeong, H.; Dunstan, D. E.; Davidson, M. R.; Goldys, E. M.; Harvie, D. J. E. *Langmuir* **2014**, *30*, 5337−5348.
(29) Lyklema, J.; Overbeek, J. *J. Colloid Sci.* **1961**, *16*, 501−512.
(30) Hunter, R.; Leyendekkers, J. *J. Chem. Soc., Faraday Trans. I* **1978**, *74*, 450−455.
(31) Protein Data Bank (PDB). http://www.rcsb.org.
(32) Inglis, D. W.; Goldys, E. M.; Calander, N. P. *Angew. Chem., Int. Ed.* **2011**, *50*, 7546−7550.
(33) Hsu, W.-L.; Harvie, D. J. E.; Davidson, M. R.; Jeong, H.; Goldys, E. M.; Inglis, D. W. *Lab Chip* **2014**, *14*, 3539−3549.
(34) Minerick, A.; Ostafin, A.; Chang, H. *Electrophoresis* **2002**, *23*, 2165−2173.